JOURNAL OF THERMOPHYSICS AND HEAT TRANSFER
Vol. 14, No. 2, April–June 2000

# Temperature Measurements by Ultraviolet Filtered Rayleigh Scattering Using a Mercury Filter

Azer P. Yalin* and Richard B. Miles†
*Princeton University, Princeton, New Jersey 08544*

**We report the development of Ultraviolet Filtered Rayleigh Scattering (UV FRS) as a diagnostic tool for measurements of gas properties. A frequency tripled, narrow linewidth, Ti:sapphire laser illuminates a sample, and Rayleigh scattered light is imaged through a mercury vapor absorption filter. The strong absorption of the filter may be used to suppress elastic background. Tuning the laser through the absorption notch of the filter is a means of probing the scattering line shape, which contains temperature information. Temperature measurements of air are shown to have uncertainties of less than 3%, whereas measurements of a weakly ionized discharge have uncertainties of less than 4%. An enhanced scattering cross section as well as nearly ideal filter properties lead to temperature sensitivities for the mercury filter in the ultraviolet which are comparable to those available with an iodine filter in the visible. The absorption for the mercury filter is modeled to be at least 5 orders of magnitude higher than for the iodine filter, meaning that stronger background suppression may be achieved.**

## Nomenclature

| | |
|---|---|
| $K$ | = magnitude of the scattering wave vector |
| $k$ | = Boltzmann's constant |
| $m$ | = molecular mass |
| $N$ | = number density of the scattering molecules |
| $n$ | = index of refraction |
| $P$ | = gas pressure |
| $S$ | = filtered Rayleigh scattering signal level at the point of maximum sensitivity, with the signal in the filter transmission normalized to unity |
| $T$ | = scattering gas temperature |
| $v_0$ | = thermal velocity |
| $Y$ | = nondimensional parameter that defines the character of the scattering lineshape |
| $\eta$ | = shear viscosity |
| $\theta$ | = scattering angle |
| $\lambda$ | = excitation wavelength |
| $\nu$ | = laser frequency |
| $\rho_0$ | = depolarization factor |
| $\sigma$ | = total scattering cross section |
| $(\,)_{\text{ideal}}$ | = indicates that the bracketed quantity is evaluated for an ideal filter |

## Introduction

OVER the past several years filtered Rayleigh scattering (FRS) has been employed as a diagnostic in a variety of gaseous environments for nonintrusive flow visualization as well as quantitative measurements of fluid properties including temperature. Nonintrusive temperature measurements are very important for improved understanding of many areas of physics, such as supersonic flows, weakly ionized plasmas, combustion processes, and the atmosphere. Our primary motivation for the work reported here is to develop the technique for plasma diagnostics. In particular, we are studying methods for producing low-temperature plasmas with electron number densities of $<\sim 10^{13}/\text{cm}^3$ (ionization fractions $<\sim 10^{-5}$). We are also interested in the propagation of shock waves through low-density plasmas. The ability to obtain one- or two-dimensional temperature and density maps of these plasmas is critical for this work.

A wide array of optical methods is available depending on the nature of the problem under investigation. FRS is attractive because, by focusing the laser to a sheet, it has the potential to provide a full two-dimensional, quantitative map of the flowfield.[1,2] Typically, spectral measurements, such as absorption and fluorescence, are path-integrated coherent anti-Stokes Raman scattering (CARS) and laser-induced thermal anemometry (LITA)[3] may be used to perform point measurements, but are inherently not well-suited for two-dimensional imaging. Raman techniques are species-specific and could possibly allow imaging, but suffer from very low signal levels. Laser-induced fluorescence (LIF) methods are amenable to imaging; however, in many cases fluorescence quenching and saturation complicate quantitative analysis. For example, one group doing point LIF measurements in an inductively coupled argon plasma found an accuracy of $\pm 80$ K ($\sim \pm 10\%$) (Ref. 4). FRS can be used to capture quantitative planar measurements of gas temperature, pressure, density, and velocity. Rayleigh scattering is a nonresonant process and thus unaffected by quenching and saturation. Furthermore, it is linear with scatterer density. Filtering the Rayleigh signal with a narrow linewidth atomic or molecular filter gives an additional temperature dependence to the signal because of the temperature dependence of the scattering line shape. In addition, the filter provides very strong suppression (modeled to be greater than $10^5$) of elastic background. Because Rayleigh scattering is an elastic process, it is often difficult to decouple the Rayleigh signal from any spurious elastic background without the use of a filter. Suppression of any nonelastic background (caused by, for example, pump lasers or sample luminosity) may be performed with conventional interference filter technologies.

In the visible region the FRS technique has already shown its utility in a variety of environments, such as for temperature measurement in combustion[5] and for velocimetry and flow visualization in high-speed flows.[1,6] This work has primarily used frequency doubled Nd:YAG sources paired with molecular iodine filters (532 nm). Some FRS work has also been done in the ultraviolet, using an excimer laser with an atomic iron filter (248 nm)[7] but with modest success because of the limitations of the seeding of the laser. Related work in the light detection and ranging (LIDAR) and other communities has paired narrow linewidth lasers and filters in the visible to infrared region, for example, an Alexandrite laser and potassium filter (770 nm)[8] or a dye laser and cesium filter (389 nm).[9,10] Additionally, rubidium (780 nm),[9] barium (554 nm),[9] magnesium (516–518 nm),[10,11] calcium (423 nm),[10] and lead (283 nm)[9] have all been considered or used as atomic filters.

The focus of this work is the extension of the FRS technique from the visible to the UV portion of the spectrum, where the scattering

Received 12 March 1999; revision received 15 September 1999; accepted for publication 1 October 1999. 

*Graduate Student, Department of Mechanical and Aerospace Engineering. Student Member AIAA.
†Professor, Department of Mechanical and Aerospace Engineering. Associate Fellow AIAA.

is stronger and the more ideal mercury vapor filter can be used. Preliminary work characterizing the mercury filter was performed in our laboratory by Finkelstein.[12] To perform temperature measurements, Rayleigh scattering from a gas sample is imaged through a mercury filter, and a model is used to fit for gas properties. The frequency dependence of the scattering cross section, as well as the absorption profile of the filter, lead to comparable temperature sensitivities in the UV than in the visible. However, the much stronger absorption of the mercury filter, compared to iodine, means that superior background suppression may be attained. In this paper the technique is explained, the mercury filter and relevant models are discussed, the experimental setup and results of temperature measurements are presented, and finally a comparison between visible and UV FRS is given. The latter comparison, as well as the discussion of the mercury filter, serve to motivate the selection of mercury as the filter material.

## FRS Technique

### Overview

A narrow linewidth laser is used to illuminate a sample volume, and the scattered light is imaged through a narrowband atomic or molecular vapor absorption filter onto a detector (Fig. 1). The amount of scattered light arriving at the detector depends on the spectral overlap of the scattered light with the filter absorption profile. The scattered light consists of an elastic background component from window scattering and stray reflections, as well as the Rayleigh light scattered from the flow. The spectral profile of the scattering intensity is termed the scattering line shape. Temperature can be determined by measuring the Rayleigh scattering line shape using the mercury vapor absorption filter. By tuning the laser, the scattering line shape is swept across the absorption filter profile causing the transmitted light to vary in intensity. Because the absorption profile of the filter is known, the transmitted intensity profile can be deconvolved to yield the Rayleigh–Brillouin line shape, from which the temperature may be determined.

### Scattering Line Shape

The light scattered by the flow has a Rayleigh–Brillouin line shape generated by the Doppler shifts associated with the thermal motion of the molecules in the sample volume. The line shape is dependent on scattering angle, temperature, pressure, and excitation frequency. The character of the line shape depends on a nondimensional quantity called the $Y$ parameter, defined by Tenti et al.[13] as

$$Y = NkT/2^{\frac{1}{2}}Kv_0\eta$$

$$[K = 4\pi/\lambda \sin(\theta/2)] \tag{1}$$

where $v_0$ is a thermal velocity, related to gas temperature and molecular mass:

$$v_0 = (kT/m)^{\frac{1}{2}} \tag{2}$$

One may manipulate this expression and use the Sutherland formula for viscosity to yield an expression for $Y$ in terms of the flow parameters appropriate for scattering from air[2]:

$$Y = 0.230[(T + 111)/T^2][P\lambda/\sin(\theta/2)] \tag{3}$$

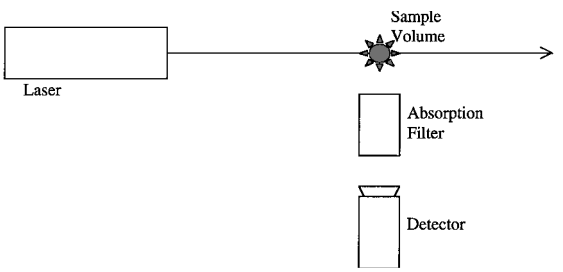


**Fig. 1 Basic setup for FRS.**

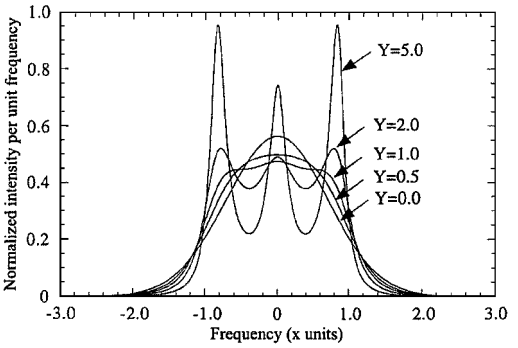


**Fig. 2 Rayleigh–Brillouin scattering profiles for various $Y$ values. Frequency is given in normalized units: $x = 2\pi v/2^{1/2}Kv_0$.**

where $T$ is in Kelvin, $P$ is in atmosphere, and $\lambda$ is in nm. For $Y$ values much less than unity, the thermal motion of the gas may be represented by a Maxwellian velocity distribution, leading to a purely Gaussian scattering profile centered at the frequency associated with the average gas motion. In such cases, entitled the Knudsen regime, the line shape is independent of pressure. The opposite extreme, corresponding to high $Y$ values, is known as the hydrodynamic regime. In this case the molecular motion is correlated, and thermally induced sound waves scatter the light. In such cases the line shape has a central Lorentzian component, caused by thermal diffusion, as well as a pair of Lorentzian sidebands, shifted out by a frequency associated with the speed of sound. In this regime the line shape has a weak pressure dependence. We are primarily interested in plasmas with subatmospheric pressures and moderate to high temperatures. Such plasmas have small values of the $Y$ parameter; however, the complete Tenti model[13] is used. Line shapes for various $Y$ parameters are shown in Fig. 2. In this work we make use of the S6 model, created by Tenti, for the Rayleigh–Brillouin line shape. This model has been successfully used by several other researchers.[1,6,9] However, even this model is not exact. The S6 model is designed for a single species of polyatomic atom while air contains a number of species. Also, the model neglects the presence of all branches of rotational Raman scattering.

### Mercury Vapor Filter

In FRS the absorption filter serves two critical purposes: background suppression and probing of spectral information. Desired filter properties are high out-of-band transmission, high in-band absorption, steeply sloping walls, and flexibility in selecting the absorption width. Mercury has an optically accessible strong ground-state transition at 253.7 nm and is well suited as a filter material. Unlike some other materials with transitions in the UV, such as iron, lead, and cesium, mercury has a low boiling point and high molar mass. The low boiling point means useful vapor number densities may be attained at relatively low temperatures. This low operating temperature together with the high atomic weight of the mercury atom (200.6 amu) reduces thermal broadening and leads to very steep filter walls if the mercury vapor pressure is kept low enough to avoid collisional broadening. In a 5-cm cell, at low vapor pressure (order 0.01 torr) lines from each of mercury's six naturally occurring isotopes form separate notches with widths up to several gigahertz and filter walls that rise from 10 to 90% transmission over hundreds of megahertz. At a higher vapor pressure (order 1 torr) the isotopic lines blend together and form a notch with a width of tens of gigahertz. In this case the filter walls are not very steep because collisional broadening is significant. Figure 3 shows absorption profiles for a 5-cm length mercury vapor cell at three different vapor pressures. The out-of-band transmission is close to 100% (neglecting filter window losses), and the in-band optical suppression is predicted to be five orders of magnitude or more. The vapor pressure is controlled by setting the temperature of a sidearm, which contains a small amount (several grams) of liquid mercury. The sidearm is immersed in a temperature-controlled liquid bath (water or mineral oil). The main body of the filter is a quartz tube of diameter 5 cm and length 5 cm. To prevent any condensation in the main

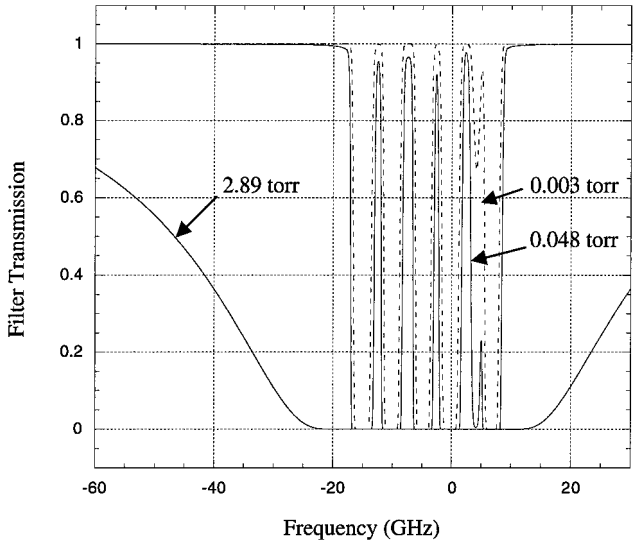


**Fig. 3 Absorption profiles for three different 5-cm-length mercury vapor filters. The three filters correspond to vapor pressures of 0.003, 0.048, and 2.89 torr, respectively.**

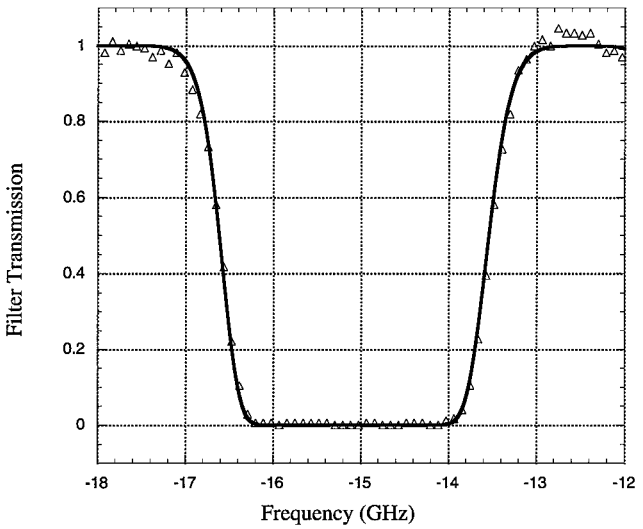


**Fig. 4 Absorption scan of the mercury vapor filter. The vapor filter has length 5 cm and a vapor pressure of 0.003 torr. The notch shown corresponds to the Hg 202 isotope and is the notch used for the presented temperature measurements.**

tube, the body of the tube is heated to a temperature slightly higher than the sidearm. By varying the sidearm temperature from ~20 to ~200 C, vapor pressures from ~0.001 to ~20 torr may be achieved. For the measurements presented in this work, a vapor pressure of 0.0030 torr was used. A model for mercury absorption has been developed in earlier work.[12] Absorption scans were performed for additional validation of the absorption model and the detection system. Figure 4 shows an experimental scan and modeled values for one of the isotopic notches.

### FRS Signal and Temperature Measurement

The FRS technique makes use of the temperature dependence of the scattering line shape in order to measure temperature. Depending on the measurement conditions, different variants of the technique may be used. At each laser frequency the amount of scattered light arriving at the detector depends on the spectral overlap of the scattered line shape (centered at the laser frequency) and the filter absorption profile. Figure 5a shows the spectral overlap of the scattered light with the filter transmission at two laser frequencies, f1 and f2. The scattered light has two components: a broadband Rayleigh–Brillouin component and a narrowband background

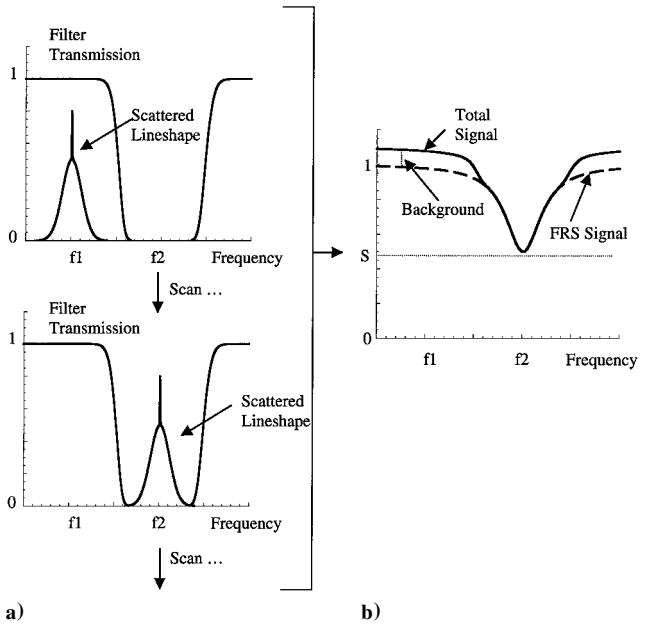


**Fig. 5 FRS signal as function of laser tuning: a) spectral overlap of the scattered light with the filter transmission at two laser frequencies, f1 and f2; b) by tuning the laser through the absorption notch the FRS signal is obtained as a function of frequency. The point in the FRS data with the maximum sensitivity to temperature is the FRS minimum, labeled S.**

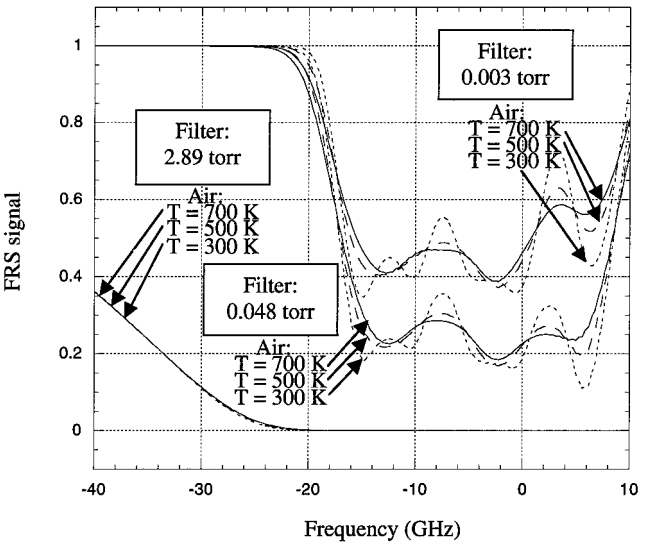


**Fig. 6 Modeled FRS signals for three different mercury vapor filter configurations for atmospheric pressure air at temperatures of 300, 500, and 700 K. The three filters correspond to those shown in Fig. 3 and are 5 cm in length with vapor pressures of 0.003, 0.048, and 2.89 torr.**

component from windows and stray reflections (shown as a sharp peak). In the most general case, by scanning the laser frequency the Rayleigh–Brillouin line shape is swept across the absorption filter profile causing the transmitted light to vary in intensity. In this manner one obtains the FRS signal as a function of frequency (see Fig. 5b). A model is used to fit the FRS data for gas properties. Of course, a laser with linewidth narrow compared to the width of the filter is required. The FRS signal is a convolution of the scattering line shape (and laser linewidth) with the filter absorption profile. Because the filter absorption profile is known, a fitting routine may be used to extract temperature from the FRS data. In this work we use a code developed by Forkey[1] for visible FRS.

Along with the fitting routine, a program to model the FRS signal has been created.[1] The program requires the filter absorption profile as one of its inputs. Figure 6 shows the modeled FRS signal as a

function of frequency for various filters and temperatures. In each case the FRS signal is normalized to unity in the filter transmission. Here it is clear that sharp filter walls are required to get significant temperature sensitivity.

A variant of the preceding technique may be used in cases where the gas is in pressure equilibrium and the pressure is known. In such cases, there is a one-to-one correspondence between temperature and density so that a single measurement may be used to determine the temperature and density simultaneously. The most practicable measurement is to take the ratio of the FRS signal at a known (reference) condition to the FRS signal at an unknown (to be measured) condition. The FRS signal model may then be used to convert the measured ratio to temperature. This method has the distinct advantage that all data are taken at a single laser frequency, meaning that by selecting the frequency to be within an absorption notch one may suppress elastic background throughout the entire measurement. This method is similar to measuring the temperature with Rayleigh scattering; however, using a filter gives the significant advantage of strong elastic background suppression.

As mentioned, by varying the filter parameters different filter absorption profiles may be obtained. In this manner an absorption filter may be tailored for a specific set of measurements.

## Experimental Setup

A schematic diagram of the experimental setup is shown in Fig. 7. A custom-built titanium sapphire laser system[12] is used as the illumination source for the UV FRS measurements. The laser is injection seeded and operates with a novel cavity locking scheme, which ensures almost transform limited, narrow linewidth single mode output. The linewidth of the third harmonic output is approximately 200 MHz, which is narrow compared to the scattering linewidth and filter absorption width, both of which are about 2 GHz. Pulse energies (in the UV) on the order of 10 mJ per pulse were used.

The third harmonic output from the laser system is delivered along the axes of a cylindrical cell, with antireflection (AR) coated windows, which houses the sample gas. A 50-cm focal length lens is used to focus the beam to a waist of $\sim 100\mu$. To minimize any background light, the beam is passed through several irises. A half-wave plate is used to ensure the correct orientation of the linearly polarized beam, and a quarter-wave plate compensates for any elliptical polarization introduced at the window. All of the beam shaping optics are AR coated. An AR coated 5-cm focal length lens is placed 8 cm from the beam and is used to image the Rayleigh scattered light at an observation angle perpendicular to the beam and cell axes. An iris of diameter $\sim 1$ mm is placed between the lens and cell and serves to define the sample region as well as to further reduce background light. The scattered light is imaged through the mercury vapor filter and then passed through an ISA H20 monochromator set to 254 nm, which acts as a broad (>1 nm) pass band filter. The monochromator rejects other colors of light caused by the pump laser or any non-Rayleigh light from the scattering volume. Finally, the scattered light is detected with an R-960 Hamamatsu photomultiplier tube (PMT).

A quartz flat is used to pick-off a fraction of the laser beam after it has passed through the cell in order to serve as a power and frequency reference. The pick-off beam is incident on a diffuser, and elastically scattered light from the diffuser is measured with a photodiode for power normalization, as well as passed through a second mercury vapor absorption filter and measured with a second PMT in order to serve as a frequency reference. The frequency axis may be established using the second mercury vapor filter by fitting the measured transmission to the modeled results. The reference vapor mercury filter was 13 cm in length and ran at room temperature. Thin-film interference filters (Corion G25-254-F) are placed in front of the reference photodiode and PMT in order to detect only the 254 nm light. These interference filters have a width of several nanometers and have a flat response over the spectral region of interest. The signals from both PMTs and the photodiode are collected using a Stanford Research Systems (SRS) boxcar unit and a personal computer. An SRS 330 preamplifier unit is used at x5 to amplify the signals from the FRS PMT as well as the photodiode. Great care was taken to ensure the linearity of the entire detection scheme.

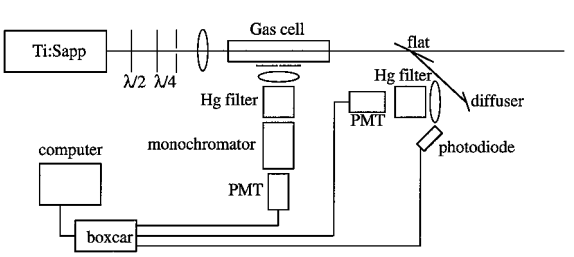


**Fig. 7 Schematic diagram of experimental setup.**

## Results

To demonstrate the technique, we initially performed temperature measurements of air. The basic procedure was to scan the laser across the filter absorption and collect the FRS signal as a function of frequency. The FRS signal was normalized using the reference photodiode, and the frequency axis was established with the reference PMT. A thermocouple inside the sample cell was used as a reference measure of temperature. Data obtained from typical scans, in this case atmospheric pressure air at $295 \pm 2$ and $330 \pm 3$ K, are shown in Fig. 8. Both data sets are normalized to one in the filter transmission. Data shown are 100 shot averages. The laser was scanned over a frequency range of $\sim 15$ GHz with a step size of approximately 40 MHz. Using the mercury absorption model and fitting routine, temperatures are extracted from the data. For example, the fits to the data in Fig. 8 returned a temperature of $304 \pm 8$ and $330 \pm 8$ K. The data shown in Fig. 8 are after background subtraction. The background signal was caused by stray elastic scatter from windows and other optics and was measured by bringing the sample cell to vacuum with the laser tuned away from the filter absorption. A test to confirm filter suppression was performed by tuning the laser to within the absorption notch and measuring the PMT signal with the cell at vacuum. In this case no signal could be measured within the dynamic range of our detection system. Air measurements have been made at three conditions: $T = 295 \pm 2$ K, $P = 1$ atm; $T = 295 \pm 2$ K, $P = 50$ torr; and $T = 330 \pm 3$ K, $P = 1$ atm. These three conditions correspond to $Y$ values of 0.39, 0.03, and 0.33, respectively. In all cases the fitting routine returned temperatures within 3% of the actual temperature. The model and data fitting procedure contains no free parameters or calibration points and does account for the laser line width as well as geometric effects.

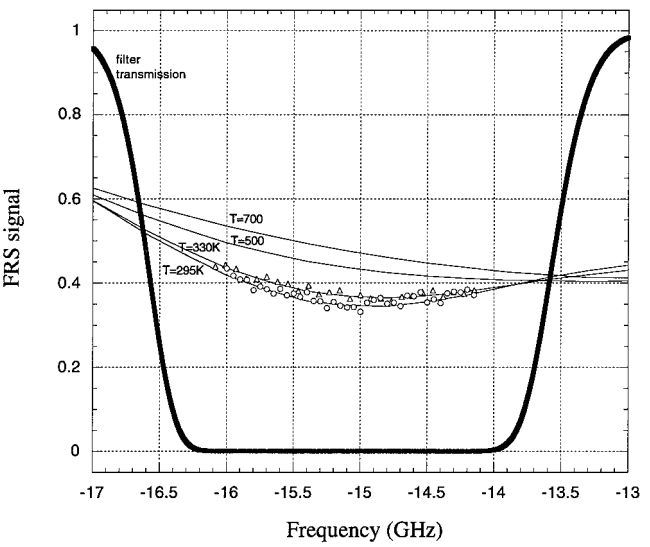


**Fig. 8 UV FRS data from air at $T = 295 \pm 2$ K, $P = 1$ atm (○) as well as data from air at $T = 330 \pm 2$ K, $P = 1$ atm (△). The modeled filter transmission profile (thick line) is shown, as well as the model fit for atmospheric pressure air at $T = 295, 330, 500$, and 700 K.**

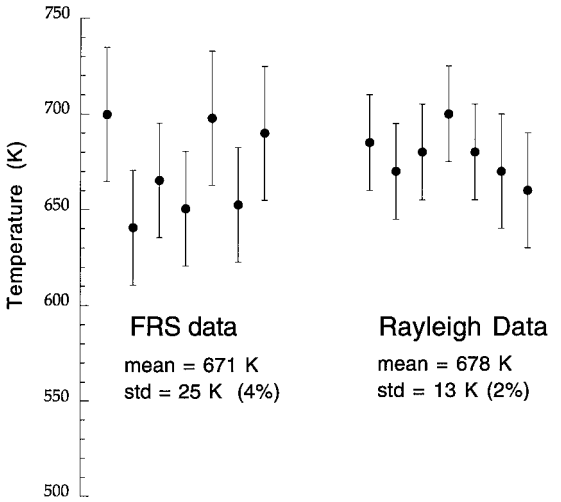


**Fig. 9 Comparison of FRS and Rayleigh scattering measurements of the axial temperature of a 50 torr, 20 mA, argon plasma.**

Uncertainties are determined by the fitting routine from noise in the data. Some error is introduced when fitting the frequency axis caused by thermal drift in the seed laser (estimated as several megahertz per minute). To remedy this, external locking schemes are being considered, for example, Ref. 14. Also, the background subtraction introduces some error, particularly at low pressure. As mentioned, background caused by stray light and window scatter was subtracted from the FRS signal. The background level may be described in terms of the pressure of a room temperature air sample that would give an equivalent Rayleigh signal in the absence of the filter. Using the AR-coated cell and the optics just described, a background equivalent to approximately 1 torr of Rayleigh scattering from air was detected.

Another series of measurements were performed at more elevated temperatures. Elevated temperatures were obtained by running a weakly ionized (ionization fraction $< 10^{-6}$) glow discharge within the sample cell. Figure 9 shows the results of FRS as well as Rayleigh measurements of the centerline temperature of a 50 torr, 20 mA argon discharge. These measurements were obtained using the constant pressure variant of the FRS approach (described in "FRS Signal and Temperature Measurement" section). The monochromator served to suppress any plasma luminosity. The laser was operated at a single frequency within the absorption notch, and the FRS signal with the discharge on was ratioed to the FRS signal at a reference temperature with the discharge off. Because the pressure is fixed, there is now a one-to-one correspondence of temperature and density so that this ratio uniquely defines the unknown temperature. Measurements with and without the filter are within experimental uncertainty. The measurements validate the UV FRS technique in this more elevated temperature range. Standard deviations of the filtered measurements are higher (4% vs 2%) caused primarily by the drift of the seed laser. Measurements by this approach, with the laser at a single frequency in the absorption notch, may also be performed in cases with a high elastic background. Because of the low ionization fraction, the change in scattering cross section caused by excited atoms, changes in scattering line shape, and any Thompson scattering can be neglected. At higher plasma temperatures, with low ionization fractions, a real-gas equation of state may be used. Measurements at higher ionization fractions will be challenging, primarily because of the dramatic variation of scattering cross section for excited atoms.

## UV vs Visible FRS

Comparing the signals obtainable with a frequency doubled Nd:YAG system to a frequency tripled Ti:sapphire system shows the benefit of working in the UV. The total scattering cross section may be given as[1]

$$\sigma = [32\pi^3(n-1)^2/3\lambda^4N^2](6+3\rho_0)/(6-7\rho_0) \qquad (4)$$

For air at 254 nm, the cross section has a value on the order of $10^{-25}$ cm$^2$ (value found by scaling data from Ref. 15). The cross section scales as inverse wavelength to the fourth power, although this is offset by the linear dependence of photon energy with frequency, resulting in a cubic dependence of the number of scattered photons for a given beam energy. Decreasing the wavelength from 532 to 254 nm (a factor of 2.09) yields a gain of 9.19 from the wavelength cubed and a gain of 1.16 caused by the increased index of refraction and depolarization.[16] Thus, for a given beam energy one has 10.7 times more Rayleigh scattered photons in going from 532 to 254 nm. Standard PMTs have comparable quantum efficiencies at 254 and 532 nm (about 25%), yielding an increase in counts by a factor of approximately 10, for a given beam energy. In practice, if one uses a UV source with 10 times lower energy per pulse than is available in the visible (e.g., 30 mJ/pulse from the third harmonic of a Ti:Sapphire system vs 300 mJ/pulse from the second harmonic of a Nd:YAG system), then the number of counts (or signal to noise) in both cases is comparable.

Another important element in comparing filters is an examination of their temperature sensitivities. An ideal absorption filter would consist of a single absorption notch with infinitely steep walls. The width of such a filter would then be adjusted for maximum temperature sensitivity for given scattering conditions. In this ideal case the point of maximum temperature sensitivity of the FRS data is the transmission minimum, which occurs when the laser is in the middle of the absorption filter (see Fig. 5). If one normalizes the FRS signal in the filter transmission to unity and labels the maximum sensitivity point as S, then one may compare the temperature sensitivities of two filters (assuming equal signal to noise) by looking at the nondimensional quantity $T\,\mathrm{d}S/\mathrm{d}T$. Using expressions from Ref. 1, one finds that an ideal filter, having infinitely steep walls, optimized for a given scatterer temperature, and assuming $Y \ll 1$, would have

$$T(\mathrm{d}S/\mathrm{d}T)_{\mathrm{ideal}} = 0.242 \qquad (5)$$

The value of $T\,\mathrm{d}S/\mathrm{d}T$ for an actual filter may be viewed as a measure of the ideality of the filter. The closer the value is to 0.242, the more ideal the filter. The primary factors in determining the temperature sensitivity of an actual filter are the slope of the filter walls, as well as the presence of other nearby absorption features. It is convenient to parameterize the problem with a nondimensional steepness, where the steepness is defined as the Doppler width (FWHM) of the scattering line shape divided by the frequency interval over which the walls turn on (e.g., the 10–90% width). Analysis shows that for steepness $>\sim 10$ one comes asymptotically close to the maximum sensitivity. Increasing the steepness beyond this value yields very little enhancement of the temperature sensitivity. Mercury and iodine filters both have steep walls (steepness $>\sim 5$) for most measurement conditions because of their high molar masses and low boiling points. Modeled values of $T\,\mathrm{d}S/\mathrm{d}T$ for mercury and iodine filters, for scattering from 50 torr air at temperatures of 400 and 800 K, are shown in Table 1. The modeled filters are 5 cm in length, and the filter temperatures (and vapor pressures) are optimized for each measuring condition.

The temperature sensitivities of iodine and mercury filters are very comparable, differing by at most 15%. The temperature sensitivity of the mercury filter is compromised by the presence of isotopes (giving a series of absorption notches), whereas for iodine the sensitivity is limited by the presence of many absorption lines as well as a background continuum absorption. For low air temperatures both filters are nearly ideal, whereas at high temperatures the presence of multiple absorption features reduces the temperature sensitivity. The

**Table 1 Comparison of modeled temperature sensitivity for mercury and iodine filters**

| Air temperature, K | Mercury cell: $T\,\mathrm{d}S/\mathrm{d}T$ | Iodine cell: $T\,\mathrm{d}S/\mathrm{d}T$ |
|---|---|---|
| 400 | 0.18 | 0.21 |
| 800 | 0.15 | 0.16 |

idea of using an isotopically enhanced mercury filter is attractive but likely not viable. Because we are using very optically thick filters, the degree of isotopic enhancement required would in general be prohibitively expensive. Some additional gain in sensitivity may also be achieved by using longer cells.

Background absorption for the mercury filter is much stronger (suppression modeled to be much greater than $10^5$ for a typical 5-cm cell) than for the iodine filter (limited to $10^5$ by background continuum absorption) so that there is a significant reduction in background noise. This is particularly important in cases where background scattering is strong compared to the Rayleigh signal, such as when windows or walls are in close proximity to the sample volume, or many particulates are present.

## Conclusion

In conclusion, we have used ultraviolet FRS to perform accurate temperature measurements in gases, using a mercury absorption filter paired with a titanium sapphire laser source. Measurements with uncertainties of 3–4% were obtained under several conditions. The absorption profile of the mercury filter, as well as the frequency dependence of the Rayleigh cross section, indicate that comparable temperature sensitivities are attained by shifting from the visible to the ultraviolet. The absorption for the mercury filter is modeled to be several orders of magnitude higher than for the iodine filter, meaning that stronger background suppression may be achieved. We are currently working to extend the diagnostic to perform spatially resolved measurements. Also, we plan to further apply the technique to temperature measurements in plasmas.

## Acknowledgments

This work was supported by the Air Force Office of Scientific Research. The authors would like to acknowledge several people whose help was critical to this work. We thank Joe Forkey for providing the code for the fitting routine and Dick Seasholtz for providing a copy of the Tenti code. The authors also thank Noah Finkelstein and Yury Ionikh for experimental guidance and Mike Sousa for his expertise in constructing optical cells.

## References

[1]Forkey, J. N., "Development and Demonstration of Filtered Rayleigh Scattering—A Laser Based Flow Diagnostic for Planar Measurements of Velocity, Temperature, and Pressure," Ph.D. Dissertation, # 2067-T, Dept. of Mechanical and Aerospace Engineering, Princeton Univ., Princeton, NJ, April 1996.

[2]Forkey, J. N., Lempert, W. R., and Miles, R. B., "Accuracy Limits for Planar Measurement of Flow Field Velocity, Temperature and Pressure Using Filtered Rayleigh Scattering," *Experiments in Fluids*, Vol. 24, No. 2, 1998, pp. 151–162.

[3]Cummings, E. B., "Laser-Induced Thermal Acoustics: Simple Accurate Gas Measurements," *Optics Letters*, Vol. 19, No. 17, 1994, pp. 1361–1364.

[4]Hebner, G. A., "Spatially Resolved, Excited State Densities and Neutral and Ion Temperatures in Inductively Coupled Argon Plasmas," *Journal of Applied Physics*, Vol. 80, No. 5, 1996, pp. 2624–2636.

[5]Hoffman, D., Munch, K. U., and Leipertz, A., "Two-Dimensional Temperature Determination in Sooting Flames by Filtered Rayleigh Scattering," *Optics Letters*, Vol. 21, No. 7, 1996, pp. 525–527.

[6]Elliot, G. S., Samimy, M., and Arnette, S. A., "A Molecular Based Velocimetry Technique for High Speed Flows," *Experiments in Fluids*, Vol. 18, No. 1–2, 1994, pp. 107–118.

[7]Andresen, P., and Golz, P., "Atomic Vapor Filter for Two-Dimensional Rayleigh Imaging Experiments with a Narrow-Band KrF Excimer Laser," *Applied Optics*, Vol. 35, No. 30, 1996, pp. 6054–6061.

[8]Bloom, S. H., Searcy, P. A., Choi, K., Kremer, R., and Korevaar, E., "Helicopter Plume Detection by Using an Ultranarrow Band Noncoherent Laser Doppler Velocimeter," *Optics Letters*, Vol. 18, No. 3, 1993, pp. 244–246.

[9]Shimizu, H., Noguchi, K., and She, C. Y., "Atmospheric Temperature Measurements by a High Spectral Resolution Lidar," *Applied Optics*, Vol. 25, No. 9, 1986, pp. 1460–1466.

[10]Gelbwachs, J. A., "422.7-nm Atomic Filter with Superior Solar Background Rejection," *Optics Letters*, Vol. 15, No. 4, 1990, pp. 236–238.

[11]Chan, Y. C., Tabat, M. D., and Gelbwachs, J. A., "Experimental Demonstration of Internal Wavelength Conversion in the Magnesium Atomic Filter," *Optics Letters*, Vol. 41, No. 14, 1996, pp. 722–724.

[12]Finkelstein, N., "An Ultraviolet Laser Source and Spectral Filters for Non-Intrusive Laser Based Diagnostics," Ph.D. Dissertation, #3015-T, Dept. of Mechanical and Aerospace Engineering, Princeton Univ., Princeton, NJ, Jan. 1997.

[13]Tenti, G., Boley, C. D., and Desai, R. C., "On the Kinetic Model Description of Rayleigh–Brillouin Scattering from Molecular Gases," *Canadian Journal of Physics*, Vol. 52, No. 2, 1974, pp. 285–297.

[14]Tsuchida, H., Ohtsu, M., and Tako, T., "Frequency Stabilization of AlGaAs Semiconductor Laser to the Absorption Line of Water Vapor," *Japanese Journal of Applied Physics*, Vol. 21, No. 1, 1982, pp. L1–L3.

[15]Shardanand, and Rao, A. D. P., "Absolute Rayleigh Scattering Cross Sections of Gases and Freons of Stratospheric Interest in the Visible and Ultraviolet Regions," NASA TN D-8442, March 1977, URL: http://techreports.larc.nasa.gov/ntrs/hget.cgi?recon?1897/3=/raid5/index/star/70%25802138%201897%20N19770012747recon1 [cited 20 March 2000].

[16]Bates, D. R., "Rayleigh Scattering by Air," *Planetary Space Science*, Vol. 32, No. 6, 1984, pp. 785–797.